Density and Phase Behaviour of (CO_2 + Methylbenzene) in Wide Ranges of Temperatures and Pressures

Yolanda Sanchez-Vicente*,[1,3] Weparn J Tay,[1] Saif Z Al Ghafri[1,2], Emmanuel C Efika,[1] J P Martin Trusler[1]

[1]Qatar Carbonates and Carbon Storage Research Centre (QCCSRC), Department of Chemical Engineering, Imperial College London, South Kensington Campus, London SW7 2AZ, UK

[2]Centre for Energy, School of Mechanical & Chemical Engineering, The University of Western Australia, Crawley, WA 6009, Australia

[3]Department of Mechanical and Construction Engineering, Northumbria University, Newcastle upon Tyne, NE1 8ST, UK

*Corresponding author: Yolanda.vicente@northumbria.ac.uk

Abstract

Knowledge of the thermophysical properties of CO_2-hydrocarbon mixtures over extended ranges of temperature and pressure is crucial in the design and operation of many carbon capture and utilization processes. In this paper, we report saturated-phase densities, compressed-liquid densities and phase behaviour of CO_2 + methylbenzene at temperatures between (283 and 473) K and at pressures up to 65 MPa over the full composition range. The saturated-phase densities were correlated by a recently-developed empirical equation with an absolute average relative deviation (AARD) of about 0.5 %. The compressed-fluid densities were also correlated using an empirical equation with an AARD of 0.3 %. The new data have been compared with the predictions of two equations of state: the predictive Peng-Robinson (PPR-78) equation of state and the SAFT-γ Mie equation of state. In both of these models, binary parameters are estimated using functional group contributions. Both models provided satisfactory representation of the vapour-liquid equilibrium and saturated-phase-density data, but the accuracy decreased in the prediction of the compressed-liquid densities where the AARD was about 2 %. The isothermal compressibility and isobaric expansivity are also reported here, and were predicted better with SAFT-γ Mie than with PPR-78. Overall, the comparisons showed that SAFT-γ Mie performs somewhat better than PPR-78 but the results suggest that further refinement of the SAFT-γ Mie parameter table are required.

1. Introduction

Carbon capture, utilisation and storage (CCUS) is a critical part of the energy mix technologies required to achieve the climate target adopted in the Paris agreement.[1] CCUS is one of the main technology to reduce CO_2 emissions from the combustion of fossil fuels in power generation and industrial processes such as steel, cement and chemicals production.[2] In the energy sector, CCUS can also facilitate the use of hydrogen from fossil fuels for heating, transport and power generation, as a new low-carbon pathway.[3] Furthermore, bioenergy with carbon capture and storage (BECCS) can contribute with net-negative emissions.[4] According to the IEA's World Energy Outlook 2018 report, the deployment of CCUS will not only significantly reduce the risk of not meeting the climate goal but will also minimise the cost of achieving the required emission reduction before 2100.[5]

At commercial scale, CO_2 can be utilised in enhanced oil recovery (EOR) with simultaneous CO_2 storage. Currently, 90% of the 31 Mt of CO_2 emissions captured and stored globally each year is for CO_2 EOR, mainly in the United States.[6] Recently, CO_2 injection to enhance shale oil/gas recovery has been explored.[7] In this process, CO_2 is injected into a hydrocarbon reservoir, raising the pressure and dissolving into the resident crude oil thereby lowering its viscosity and mobilising flow to the production wells. Depending upon the reservoir structure, a substantial amount of the injected CO_2 may be stored permanently, while CO_2 separated from the produced oil may be re-circulated.[8] The performance, economy and safety of CO_2 EOR strongly depend on the phase behaviour and thermophysical properties under the prevailing high-temperature and high-pressure conditions in which the CO_2 contacts the oil. The latter is of course composed of a very large number of different hydrocarbons. The density and phase behaviour of these systems strongly influence the quantity of CO_2 that can be sequestrated in a hydrocarbon reservoir. Furthermore, the reservoir fluid-flow model and the calculation of CO_2 oil swelling relies on saturated-phase and compressed-fluid densities.[9] Additional, such data are very important in the design of downstream processing and in numerous other industrial processes including supercritical-fluid extraction.[10]

Numerous thermodynamic models are available to calculate properties of carbon dioxide-hydrocarbon mixtures. Among of them, cubic equations states (CEOS), such as the Peng-Robinson[11] and Soave-Redlich-Kwong equations,[12] are widely used in petroleum and chemical engineering applications. Traditional CEOS contain binary parameters that must be optimized against experimental data for each binary sub-system. Although, in many cases, CEOS can describe phase equilibria quite accurately, they are often quite inaccurate for density and derivative properties such as heat capacity and sound speed. In contrast, multi-fluid Helmholtz Equations of State (MFHEOS), especially the GERG-2008 EOS of Kunz and

Wagner, are able to represent accurately phase-equilibria, density and derivative properties provided that the model is fully parameterised against extensive experimental data.[13, 14] The GERG-2008 model was developed for natural gas and similar mixtures containing up to 21 components, including CO_2, normal alkanes up to C_{10} and several other components. Therefore, the capabilities of this model to describe the properties for CO_2-hydrocarbons systems are of interest.[15-17] Recently, we have measured phase behaviour, compress- fluid densities and saturated-phase densities for the binary system (CO_2 + n-heptane) at temperature from (283 to 473 K) with pressure up to 68 MPa. We compared the experimental data with the predictions of the GERG-2008 model and found that it predicts the vapour-liquid equilibrium (VLE), the saturated-phase and compressed-fluid densities no better than the SAFT and Peng-Robison models.[18] The (CO_2 + decane) system has been studied by Kandil et al.[19] These authors reported that the GERG equation predicted densities within about 1%; however, they found the CEOS were superior for the prediction of the bubble pressures.

Models such as the Peng-Robinson or GERG-2008 equations of state require significant amount of experimental data, at representative temperatures and pressures, to determinate the full set of binary parameters required in a multi-component mixture, such as CO_2 + oil. For that reason, more predictive approaches have been investigated. Jaubert and co-workers proposed the predictive Peng-Robinson equation (PPR-78)[20] and also a predictive version of the Soave-Relich-Kwong equation (PSRK)[21]. These predictive methods use a group contribution approach in which the temperature-dependent binary interaction parameter is calculated on the basis of the functional groups into which each molecule can de decomposed. Jaubert and co-workers initially published the PPR-78 with 6 functional groups;[20] this was soon expanded to 21 groups, including CO_2[22] and aromatic groups,[23] and the most recent version includes a total of 40 functional groups and individual molecules.[24] The reliability of this EoS has been tested in comparison with phase behaviour and densities of multicomponent mixtures for CO_2 and hydrocarbons.[25, 26] In recent years, group-contribution versions of the Statistical Associating Fluid Theory (SAFT) have been developed. For example, in the SAFT-γ Mie equation of state the Mie potential (generalised Lennard-Jonesium) is used to represent interactions between functional groups that represent the molecules. The thermodynamic properties of numerous systems have been successfully predicted by SAFT-γ Mie.[27, 28] However, little experimental data are available to allow tests of PPR-78 and SAFT-γ Mie for mixtures containing CO_2 and hydrocarbons over substantial ranges of temperature and pressure. In this context, we have initiated a program to study the phase behaviour, saturated-phase and compressed-fluid densities of binary mixtures containing CO_2 and hydrocarbons, including new experimental measurements over extended ranges of pressure and temperature. The objective of this program is to permit testing of these thermodynamic

models, and potentially their optimisation, in an extensive range of condition. In previous work, we have reported the phase behaviour and both compressed-fluid and saturated-phase densities for the binary system (CO_2 + n-heptane) at temperatures from 283 K to 473 K and pressures up to 68 MPa.[18] In this paper, we report new phase behaviour and density measurements of (CO_2 + methylbenzene) systems from (283 to 473) K and pressures up to 65 MPa. Methylbenzene was selected as a representative of the aromatic hydrocarbons present in crude oil. Most studies in the literature relate to binary systems of (CO_2 + alkanes), and far fewer data exist for (CO_2 + aromatics). The phase equilibria for the (CO_2 + methylbenzene) system have been reported by several authors at temperatures from (283 to 572) K and pressures from (10 to 70) MPa.[29-41] However, density data for this binary system are lacking in the literature. To our knowledge, there are only two sets of compressed fluid density data available: the study of Pohler and Kiran, for mixtures containing (75 to 95) mol % CO_2 at temperatures from (323 to 423) K and pressures from (10 to 70) MPa;[42] and the study of Wu et al., for 90 mol % CO_2 at temperatures from (313 to 393.2) K and pressures from (4.19 to 43) MPa.[43] Saturated-liquid densities have been reported by Chang et al. at temperatures from (290.8 to 310.1) K and pressures up to 12.43 MPa[32] and by Zirrahi et al. at temperatures from (298.15 to 363.15) K and pressures up to 5.1 MPa.[44] Therefore, the present work significantly extends the experimental range of density data for the (CO_2 + methylbenzene) system to include high-temperature and high-pressure states relevant to CO_2-EOR. The measurements were made out in specialised apparatus and are supported by a detailed assessment of uncertainty.[45-48] The new experimental data are compared with predictions from the SAFT-γ Mie and PPR-78 equations of state. The data could also be used to optimise binary interaction parameters in either traditional CEOS or the MFHEOS for CO_2 + hydrocarbon system.

2. Materials and Methods

2.1 Materials

Pure deionized water (electrical resistivity > 18 MΩ·cm at T = 298.15 K) was obtained from a Millipore purification apparatus and was used for calibration purposes. Carbon dioxide and helium were sources from BOC with mole-fraction purities ≥ 0.99995 and ≥ 0.99999, respectively. HPLC grade of methylbenzene was supplied by Sigma-Aldrich with a mole fraction purity greater than 0.999. No analysis or further purification was attempted except that methylbenzene and water were degassed under vacuum with stirring immediately prior to use.

2.2 Phase Behaviour Measurement Apparatus

The phase behaviour of CO_2 + methylbenzene was measured with the VLE apparatus detailed previously by Al Ghafri et al.;[28] therefore, only a summary is given here. The apparatus consisted of a variable-volume cell, high-pressure syringe pumps, servo-control system, and a heating system. The cell was equipped with a movable piston, to permit variation of the volume, and a sapphire window for visual observation of the sample. A servomotor was used to drive the piston with a control system to allow simple operation of the apparatus via a host PC. A pair of high-pressure syringe pumps was used for quantitative injections of the two pure substances into the cell. A calibrated flow-through pressure transducer (DJ Instruments, model DF2) with an internal volume of only 12 µL was used to measure the pressure. The temperature of the cell was measured with a calibrated 4-wire Pt100 sensor which was inserted into a blind axial hole in the cell wall. The equilibrium cell was surrounded by an aluminium heating jacket, approximately 10 mm thick, fitted with heaters and an additional Pt100 thermometer to facilitate temperature control. Operating with a PID controller, the cell temperature was maintained constant to within ±0.01 K. Except for the operation of injecting fluids, the operation of the apparatus was fully automated. The apparatus was rated for operation at pressures up to 40 MPa and at temperatures up to 423.15 K.

The measurements were performed using the synthetic-visual method. Initially, a measured amount of methylbenzene was injected into the previously evacuated cell. Next CO_2 was injected into the cell in steps. After each injection, the composition of the fluid in the cell was calculated from the cumulative amounts of the two pure substances injected from the pumps, after allowance for the amounts held up in the interconnecting tubing. The pressure was then adjusted by moving the piston until a single homogenous phase was obtained and the contents were allowed to equilibrate with stirring. The time required to reach equilibrium was typically about one hour under continuous stirring. Starting from the homogeneous state, the pressure was decreased stepwise, with further periods for equilibration until a bubble- or dew-point was observed. Typically, CO_2 was then added to change the composition and a new measurement was started. The whole procedure was repeated at different temperatures to build up the isotherms. On each isotherm, the critical pressure and composition were identified by fitting the near critical data as detailed in the Supporting Information. The experimental procedure has been described in greater detail previously.[26]

2.3 Saturated-Phase Density Measurement

The saturated liquid-phase and vapour-phase densities were measured using an experimental apparatus comprising an equilibrium cell, two vibrating-tube densimeters (VTD, Anton Paar, DMA-1400), and two automated syringe pumps. A detailed description of the equipment can

be found in our earlier papers.[18, 45] The VTDs (one for each phase) were connected to the top and bottom ports of the equilibrium cell. Temperature control was achieved by placing the equilibrium cell and the two VTDs in an oven. Each densimeter was connected to a syringe pump (SP) via a 6 mL coiled tube. The pressure was measured by means of calibrated transducers (Sensata Technology, model 101HP2) connected to each pump. The temperatures of the two VTDs and the equilibrium cell were each measured with a Pt100 thermometer. The apparatus supported working pressures up to 70 MPa and temperatures up to 473.15 K.

Prior to the measurements, the apparatus was evacuated and flushed repeatedly with CO_2. Then, half of the cell volume was filled with methylbenzene injected from the bottom pump. Next, CO_2 was injected from the top pump to achieve a target pressure and the mixture was stirred until equilibrium was achieved. To initiate a measurement, a saturated-liquid sample was first drawn from the bottom of the equilibrium cell into the bottom VTD. This was accomplished by slowly retracting the bottom syringe pump, while maintaining the system pressure constant by action of the top pump (operating in pressure-control mode). When about 4 mL of liquid had been transferred, the lower syringe pump was halted and the oscillation period of the lower VTD, pressure and temperature were averaged over a period of about 3 min. The criterion adopted for accepting a measurement was that the standard deviation of the period was less than 0.01 μs. A similar procedure was adopted to measure the vapour-phase density: after re-mixing the cell contents, about 4 mL of vapour phase was transferred into the top VTD at constant pressure. Once the density of both phases had been measured, additional CO_2 was injected to increase the pressure and a new measurement was started. After completing an isotherm, the pressure was reduced to the minimum by venting the components. In previous work for the CO_2 + n-heptane system[18], the reproducibility of the saturated phase densities was tested by re-measuring a data at T = 323 K. Following a similar procedure for the CO_2 + methylbenzene system, we estimated that the reproducibility of our measurements is 1 kg m^{-3}.

2.4 Compressed-Fluid Density Measurement

Compressed-liquid density measurements were carried out with the experimental set-up described previously.[18, 47] The experimental set-up consisted of a vibrating-tube densimeter (Anton-Paar, DMA HP), a manual syringe pump (DH Budenburg), temperature and pressure sensors and a variable-volume cell. The temperature was controlled and measured by the thermostat and temperature sensors built into the DMA HP with an associated uncertainty of 0.01 K. The period of oscillation of the vibrating-tube was measured with a resolution of 0.001 μs. The syringe pump allowed the sample pressure to be adjusted. The pressure was

measured with a relative uncertainty of 0.05 % using a pressure transducer (Keller model 33 X) installed in the connecting tubing.

The binary mixtures of CO_2 + methylbenzene at four compositions were prepared gravimetrically in a variable-volume cell. This cell contained a piston which segregated the vessel into sample- and pneumatic-fluid compartments. A magnetic stirrer bar was placed in the sample side to agitate the mixture. Before sample preparation, the variable-volume cell was rinsed with solvent and dried under vacuum. Liquid methylbenzene was then transferred to the cell from an HPLC pump operating in dispensing mode (Knauer, Smartline S1000) and CO_2 was added from a supply cylinder fitted with a dip tube that permitted withdrawal of liquid. During this second transfer, the mass of the cell and its contents were monitored on a large-capacity balance which allowed the amount of CO_2 to be approximately controlled. The precise mass of each component was determined by weighing the cell, before and after each addition, on an analytical balance (Mettler Toledo, model PR5003) with 5 kg capacity and 0.001 g resolution. The resulting standard uncertainty of the mole fraction of CO_2 was estimated to be $\leq 10^{-5}$. Following preparation of the mixture, the pressure was increased to above the bubble point, by admitting nitrogen into the pneumatic compartment, and stirred for approximately 2 hours.

The entire densimeter and other parts of the fluid system were flushed with solvents, purged with gas and finally evacuated for drying. The homogenised mixture was then injected into the densimeter apparatus while maintaining the pressure in the variable-volume cell constant with nitrogen. Once the pressure in the densimeter apparatus was equalised with the variable-volume cell, a few mL of sample was slowly discharged at constant pressure to ensure that any inhomogenous mixture, resulting from flashing at the initial low pressure, was expelled from the densimeter tube. Finally, the densimeter was isolated from the variable-volume cell and the measurements started with further adjustments of pressure being accomplished using the manual syringe pump. Densities of binary mixtures of methylbenzene and carbon dioxide were measured from just above the bubble pressure to 68 MPa and at temperatures from (298.15 to 473.15) K in intervals of 25 K. The temperature T = 283.15 K was also studied. An additional measurement at the initial pressure on each isotherm was made as a test of repeatability; no significant differences from the initial density measurement were in fact observed.

2.5 Calibration and uncertainty

The density, ρ, related to the period of oscillation, τ, in a vibrating-tube densimeter is given by the relation:

$$\rho(T,p) = A(T,p) - B(T,p)\tau^2 \quad , \tag{1}$$

where *A* and *B* are calibration parameters determined by measurements with fluids of known densities. The calibration of the densimeters in the saturated-phase density apparatus, was performed under vacuum at each experimental temperature and in methylbenzene over the entire temperature and pressure range. The density of methybenzene was calculated from the equation of state of Lemmon and Span[49], which has an uncertainty of 0.05 %. *A* and *B* were represented as functions of temperature and pressure using expressions based on the physical properties of the vibrating-tube as detailed in an earlier paper.[50, 51] The densimeter used for compressed-fluid density measurements was calibrated with vacuum, helium and water over the full temperature and pressure range of interest. The densities of helium and water were calculated from wide-range equations of state with uncertainties of between 0.0005 % and 0.05%, depending upon the state point.[52-54] In this case, *A* and *B* were represented by polynomial functions of pressure and temperature.[18, 47]

The temperature sensors were calibrated over the temperature range (273 to 473) K on the ITS-90 using a triple-point-of-water cell and by comparison with a standard 25 Ω PRT immersed in a stirred oil bath. The pressure transducers were calibrated against a reference quartz-crystal pressure gauge (Fluke, model PPCH-G 70 M) with a relative uncertainty of 0.02 % of the full-scale pressure (i.e. 14 kPa) as described previously.[26, 45]

The overall standard uncertainty for the densities and phase equilibrium measurements was performed according to the *Guide to the Expression of Uncertainties in Measurements* (GUM).[55] The overall expanded uncertainty for compressed-fluid densities and saturated-phase densities was estimated to be ≤ 1 kg·m^{-3} and ≤1.5 kg·m^{-3}, respectively, for all state points. The uncertainties calculated were based on the temperature and pressure control and the repeatability of the measurement. It has to be noted that measurements made close to the critical region were associated with a slightly higher uncertainty. The uncertainty of the bubble- and dew-pressures depends mainly on the visual observation of the bubble- or dew-point condition. Except close to a critical point, bubble points were observed easily with an uncertainty of less than 0.2 MPa. It was more difficult to observe dew points by means of isothermal volume changes and only a few points at high pressures were measured with expanded uncertainties of between 0.3 MPa and 0.4 MPa. These estimated uncertainties do not include errors associated with impurities originally present in the sample or with unexpected sample contamination. The uncertainty analyses have been reported in greater detail in our early papers.[28, 45, 47] The calculated uncertainties, together with the experimental data are shown in Tables S1, S3, S4 in the Supporting Information.

3. Experimental results and discussion

Phase equilibrium of the binary mixture of CO_2 + methylbenzene was investigated at temperatures between (298 and 423) K and at pressures up to 18 MPa. The saturated-phase densities were measured at pressure up to the critical for temperatures ranging from (298 to 448) K. The compressed-fluid densities were reported at pressures up to 68 MPa for temperature from (283 to 473) K. The densities of pure methylbenzene and CO_2 were also measured in this work and are given in Table S4. The results for pure CO_2 and pure methylbenzene are compared in Figures S1 (CO_2) and S2 (methylbenzene) in the Supporting Information with values calculated using multi-parameter reference equations of state.[49, 56] For methylbenzene, the data agree to within the combined uncertainty of the experiment and the equation of state while, in the case of CO_2, 90% of the experimental data fall within the combined uncertainty. These figures further validate the experimental procedure and the reported uncertainties for the case of compressed-fluid densities.

3.1 Phase equilibrium

Bubble and dew points were measured at temperatures of 298 K, 323 K, 373 K and 423 K and at pressures up to 18 MPa. The experimental data, given in Table S1 in the Supporting Information, are plotted in Figure 1. Also shown in Figure 1 are the data reported by Chang et al.,[32] Lay et al.,[35] Lay,[40] Prausnitz and Benson,[29] Fink and Hershey,[38] Tochigi et al.,[33] Kwon et al.,[48] Lazzaroni et al.,[30] Kim et al.,[37] Wu et al.,[41] and Sebastian et al.[31] Good agreement is observed between the present results and most of these data from the literature. The critical points were also determined and the values of the critical pressure and composition are given in Table S2 in the Supporting information. The critical locus is plotted in Figure 2 in comparison with data from the literature.[57] Again, good agreement is observed. Additionally, Figure 2 shows the *p*, *T* projection of the critical curve obtained, using the numerical technique of Heidemann and Khalil,[58] from the Peng-Robinson equation of state,[11] and also the critical curve predicted by SAFT-γ Mie.[27] CO_2 + methylbenzene exhibits Type II phase behaviour according to the classification of Scott and van Konynenburg[59, 60], with a continuous vapour-liquid critical locus connecting the critical points of the two pure components, as well as a three-phase vapour-liquid-liquid equilibrium (VLLE) line at low temperatures terminating at an upper-critical end point located close to the critical point of CO_2. In general, SAFT-γ Mie model described the critical curve relatively better than Peng-Robinson across the calculated temperature range.

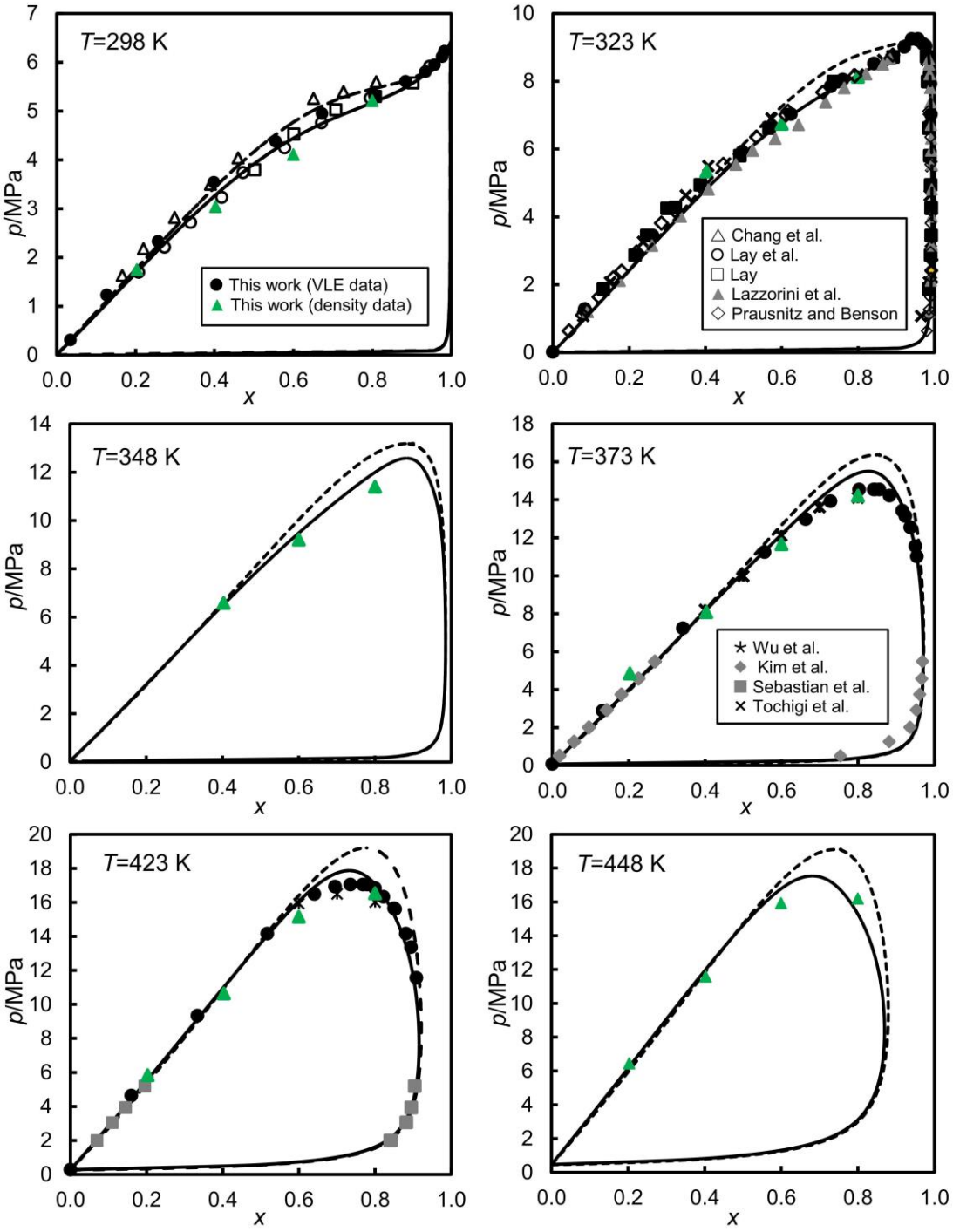

Figure 1. Vapour-liquid equilibrium for (1−x) C_7H_8+xCO_2 system at several temperatures. The symbols represent experimental data obtained in this work and literature[29, 31-35, 37, 40, 41]. Prediction from PPR-78 EoS (dashed line) and SAFT-γ Mie (solid line).

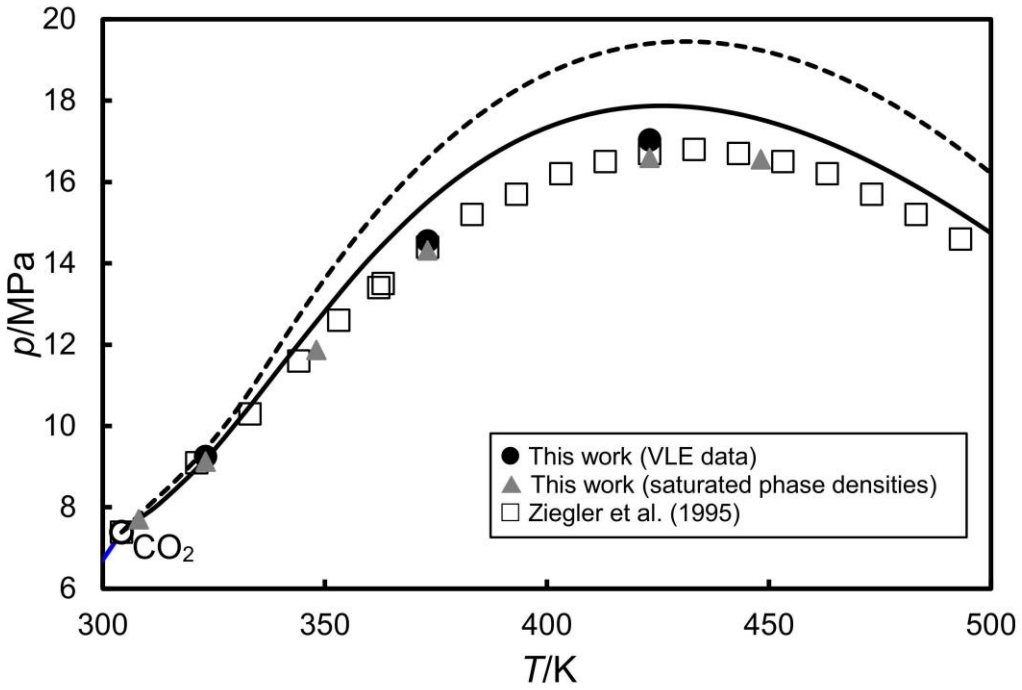

Figure 2. Critical locus for C_7H_8 + CO_2 system. The symbols represent experimental data obtained in this work and literature[57]. Dashed and solid lines are obtained with the method of Heidemann and Khalil [58] and the Peng–Robinson equation of state[11] and SAFT-γ Mie equation, respectively

3.2 Saturated-phase densities

Densities of saturated vapour and liquid phases were measured at seven temperatures, T = (298, 308, 323, 348, 373, 423 and 448) K, up to the critical pressures. The experimental data, given in Table S3 in the Supporting Information, are plotted in Figure 3. The densities of pure methylbenzene and CO_2 were also plotted in Figure 3.

At the two lower temperatures investigated, the bubble-point densities have a positive initial slope with respect to pressure, pass through a maximum and then decrease smoothly towards the critical density. At higher temperatures, the bubble-point densities decreased monotonically with pressure along an isotherm. The dew-point densities increased monotonically with increasing the pressure along each isotherm towards the critical density. The experimental saturated-phase density data at temperatures of 298 K and 308 K are compared with those reported Chang et al.[32] and Zirrahi et al.[8] in Figure S4 in the Supporting Information. Good agreement can be observed.

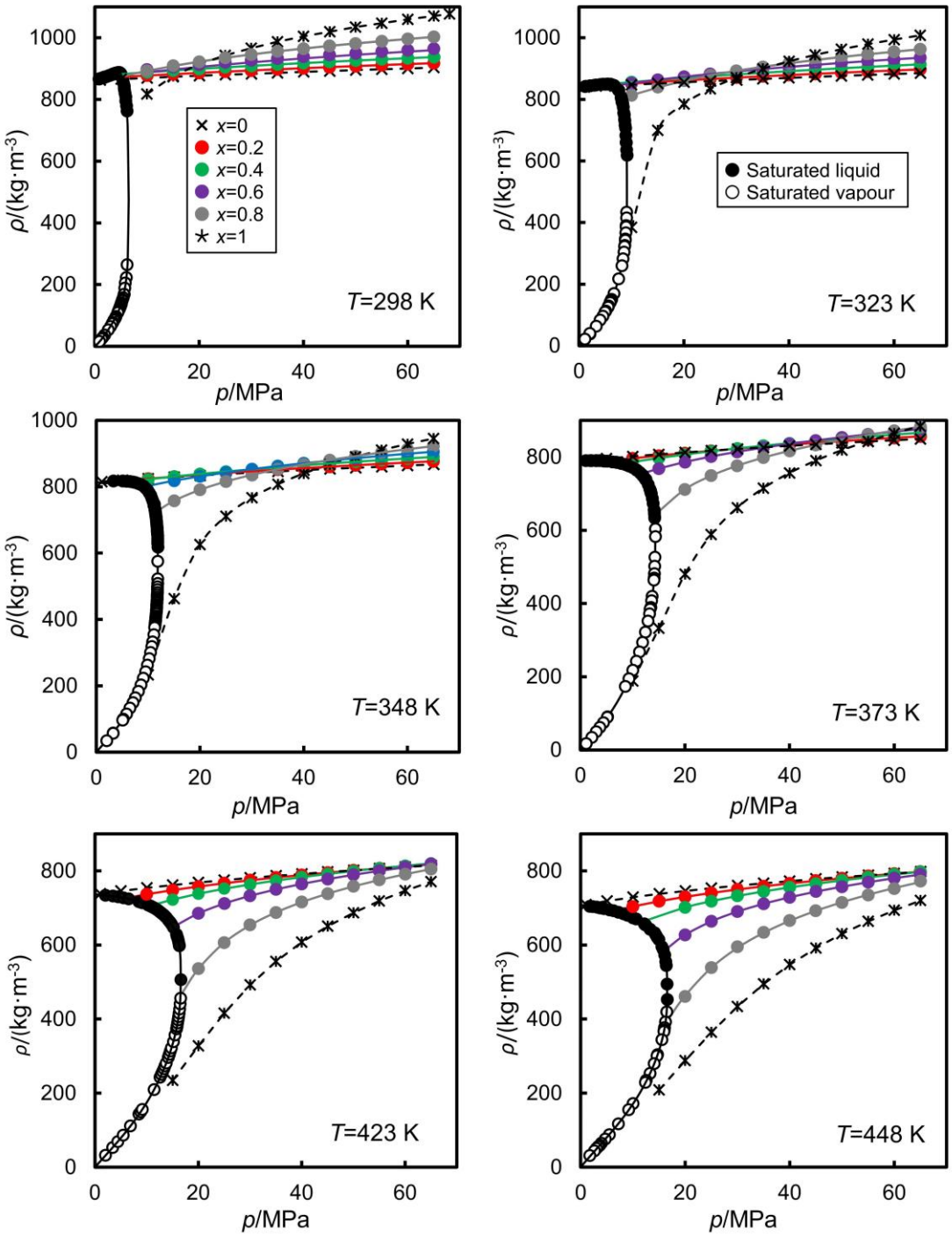

Figure 3. Experimental saturated-phase densities (black circle) and compress-fluid densities (coloured circle), ρ, of ((1−x) C_7H_8+xCO_2) system versus pressure p, at several temperatures. Black curve determined from Equation (4) with the parameters in Table S8. Coloured lines and black dashed lines are obtained using Equation (5) and parameters from Table S9.

3.3 Compressed-Fluid densities

Compressed-fluid density measurement were carried out as a function of pressure along nine isotherms at T = (283, 298, 323, 348, 373, 398, 423, 448 and 473) K and at pressures up to 65 MPa for nominal mole fractions of 0.2, 0.4, 0.6 and 0.8. The experimental densities together with the standard uncertainties are listed in Table S4 in the Supporting Information. In Figure 3, experimental compress-fluid densities are plotted against pressure along isotherms. At these conditions, the mixtures are in either liquid or supercritical-fluid states. As expected, with fixed composition, the density increased with increasing pressures but decreased with increasing temperatures. A crossover effect in the mixture densities is observed with increasing CO_2 mole fraction x, whereby $(\partial\rho/\partial x)_{T,p}$ changes from negative values at low pressures to positive values at high pressures. The crossover point is observed to shift towards higher pressures with increasing temperature, moving above the experimental pressure range at $T \geq 423.15$ K. This crossover effect can be explained by the difference in compressibility between the pure components. The density crossover phenomena in CO_2-hydrocarbon mixtures was also observed in our earlier work with CO_2 + n-heptane system.[18] However, in the CO_2 + n-heptane system, the crossover effect occurred at temperature higher than 323 K.

The density data reported here cover very large ranges of temperatures, pressure and composition and are characterised by small relative uncertainties on the order of 0.1 %. The only literature data with which to compare are those reported by Pohler and Kiran at temperatures between (323 and 423) K and at pressures up to 70 MPa.[42] These measurements are restricted to mole fractions of CO_2 between 0.74 and 0.94 and are characterized by relatively large uncertainties of up to 1.2 %. To facilitate comparison with our results at x = 0.8, we performed linear interpolations with respect to mole fraction and pressure in the data reported by Pohler and Kiran; the results are then compared in Figure S3 in the Supporting Information. We observe that the interpolated literature density data are generally higher than our results on every isotherm. The average absolute relative deviation, Δ_{AARD}, between both sets of data is 1.8%. The compressed fluid density was also reported by Wu et al. at temperatures from (313 to 393.2) K and pressures from (4.19 to 43) MPa for x = 0.90.[43] Since their data were reported at different composition, pressure and temperature from our measurements, direct comparison was not performed.

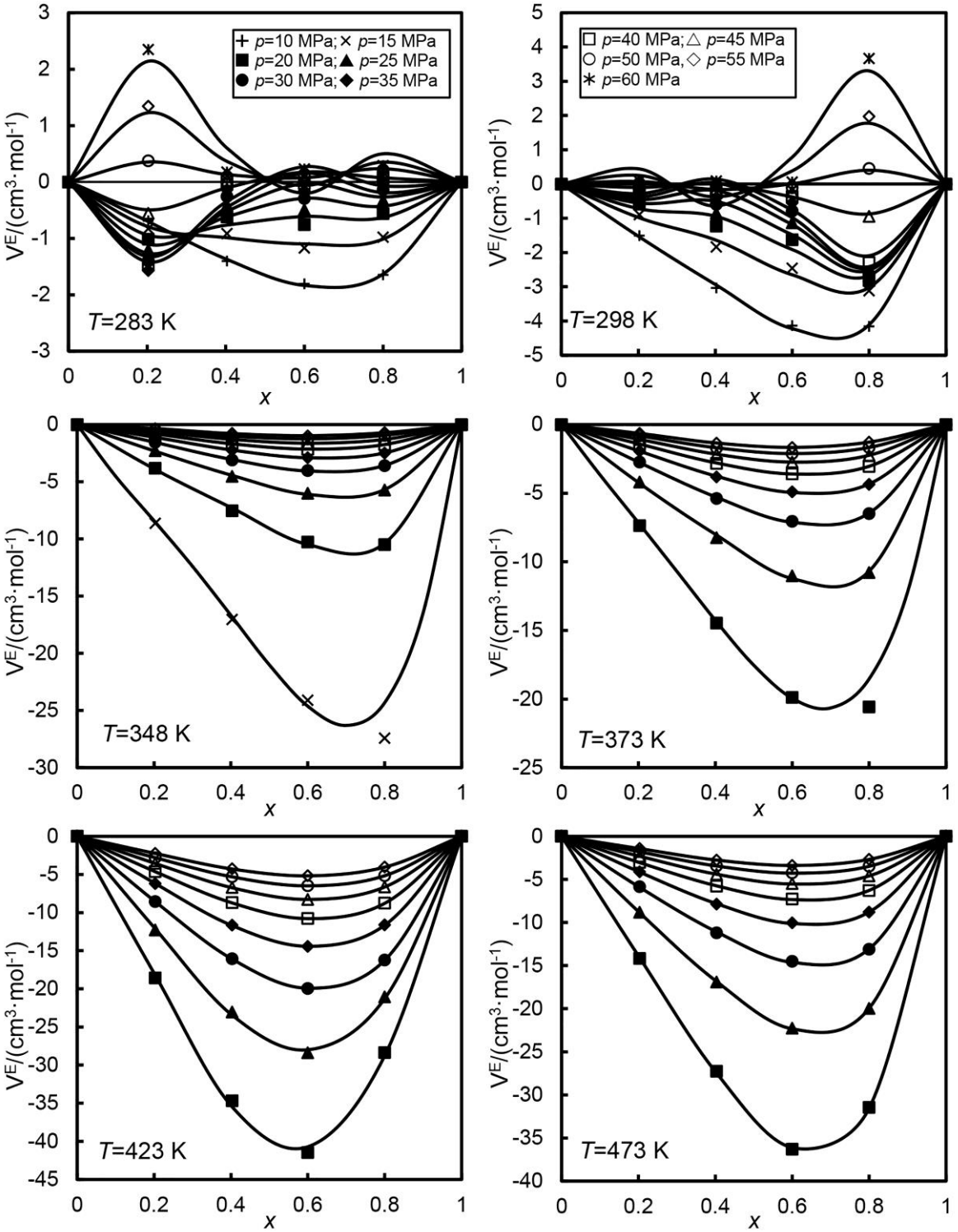

Figure 4. Excess molar volume V_m^E of ((1−x) C_7H_8+xCO_2) versus the mole fraction, *x,* of CO_2 at several temperatures and pressures. Curves are calculated using the Equation 3 and parameters in Table S5**.**

3.4 Excess molar volume

We calculated excess molar volumes (V_m^E)from the experimental compressed-fluid densities by means of the following equation:

$$V_m^E = \frac{M_{mix}}{\rho_{mix}} - \left[\frac{xM_1}{\rho_1} + \frac{(1-x)M_2}{\rho_2} \right] . \quad (2)$$

Here, x is the CO_2 mole fraction, M is the molar mass and ρ is the density; subscripts mix, 1 and 2 denote properties of the mixture, carbon dioxide and methylbenzene, respectively. Figure 4 shows plots of V_m^E as a function of x on six isotherms. At low temperatures, V_m^E displays a complex sigmoidal variation with composition, whereas for $T \geq$ 348 K, V_m^E is negative over the entire range of composition. At temperatures of 298.15 K and 283.15 K, V_m^E has negative values at pressures between 10 and 45 MPa over the full composition range whereas, at higher pressures, V_m^E presents positive and negative values depending upon composition (Figure S8 shows enlargements of the V_m^E data at T = 298.15 K and T = 283.15 K). The negative values of V_m^E observed at T = 298.15 K over most of the composition and pressure ranges indicate that CO_2 molecules are able to insert themselves into the free volume between the methylbenzene molecules without greatly expanding the original volume occupied by the methylbenzene. This situation is reversed at high-density states, corresponding to high pressure and low CO_2 mole fraction, where insertion of CO_2 molecules requires a much-larger increase in the liquid volume. Generally, at $T \geq$ 348 V_m^E tends to increasingly negative values as temperature increases and pressure decreases. The turning points for V_m^E as a function of x at constant T and p generally occur in the composition range $0.6 \leq x \leq 0.8$ and the most negative values of V_m^E are observed in regions where CO_2 behaves as a gas-like fluid while the mixture is liquid. In contrast, for states in which pure CO_2 is a liquid, the excess volumes showed moderate values. The densities of pure components in relation to the mixture densities are shown in Figure 3.

The excess molar volumes have been correlated with Redlich-Kister polynomials in the following form:

$$V_m^E = x(1-x)\sum_{i=1}^{3} A_i (2x-1)^i . \quad (3)$$

Here, A_i are adjustable parameters which were fitted to the data at each temperature and pressure. These polynomials are plotted along with the experimental data in Figure 4 and a good fit is generally observed. The goodness of the fit is illustrated by the value of Δ_{AAD} which is 0.2 $cm^3 \cdot mol^{-1}$ for all data points. The parameters A_i are given in Table S5 in the Supporting Information.

3.5 Further Analysis

Both the saturated liquid-phase and vapour-phase densities were correlated isothermally using the following empirical correlation developed previously:[55]

$$\left.\begin{aligned} \rho_{\mathrm{L}} - \rho_{\mathrm{V}} &= \sum_{i=1}^{2 \text{ or } 3} A_i (p_{\mathrm{c}} - p)^i + C(p_{\mathrm{c}} - p)^{\beta} \\ \rho_{\mathrm{L}} + \rho_{\mathrm{V}} &= 2\rho_{\mathrm{c}} + \sum_{i=1}^{2 \text{ or } 3} B_i (p_{\mathrm{c}} - p)^i + D(p_{\mathrm{c}} - p)^{\beta} \end{aligned}\right\} . \qquad (4)$$

Here, ρ_{L} and ρ_{V} are the saturated liquid-phase and saturated vapour-phase densities, respectively, ρ_{c} is the critical density, p_{c} is the critical pressure, $\beta = 0.325$ is a universal critical exponent, and A_{i}, B_{i}, C and D are parameters. These parameters, together with the values of ρ_{c} and p_{c} were adjusted to minimise the overall sum square of the deviations of the experimental data from the correlation using the Lenvenberg-Marquardt algorithm. At $p = 0$, ρ_{L} was set equal to the density of pure liquid methylbenzene at $p \rightarrow 0$, while ρ_{V} was set to 0. The parameter values at each temperature and the corresponding absolute average deviation are listed in Table S8. Deviations plots of the experimental densities from the correlation are also plotted in Figure S5. The Δ_{AAD} and Δ_{AARD} were less than 2 kg·m^{-3} and 0.5 %, excluding data very close to the critical point. This correlation allows precise estimation of the critical pressure. The critical points obtained from the saturated phase density measurements are shown in Figure 2 and they were found to be in close agreement with previous data obtained by direct observation in this work and in the literature.[57]

The compressed-fluid densities were fitted with the following implicit empirical function which relates pressure and density at constant temperature and composition:

$$p = A\rho + (B/\delta)(\rho - \rho_{\mathrm{r}})^{\delta} \quad . \qquad (5)$$

Here, $\delta = 4.82$ is a universal critical exponent and A, B and ρ_{r} are adjustable parameters which were obtained in a non-linear regression according to the Lenvenberg-Marquardt algorithm. The curves obtained with Eq. (5) are plotted in Figure 3 and show good agreement with the experimental data. The fitting parameters and the values of Δ_{AAD} and Δ_{AARD} are given in Table S9 in the Supporting Information, while Figure S5 shows the deviations of the data from the fitting function. It was found that the empirical correlation represented the data with overall Δ_{AAD} and Δ_{AARD} values of about 0.05 MPa and 0.25%, respectively.

Combining both sets of experimental density data, we were able to determine the bubble pressures for four compositions and six isotherm. The bubble pressures were found by

calculating the intersection point between the compressed fluid densities, with known composition, represented by Eq. (5), and the coexistence curve, represented by Eqs (4). The bubble pressures so determined are shown in Figure 1 and are given in Table S10 in Supporting Information. As can be seen from figure, the bubble pressures determined in this way agreed with the bubble pressures observed in the VLE measurements to within ± 0.2 MPa. This level of agreement is comparable to the uncertainty of the VLE data.

4. Modelling

The VLE data, and the densities of the compressed fluid and the saturated phases are compared with the predictions of two equations of state: PPR-78 and SAFT-γ Mie. Both equation of state are fully predictive and we did not fit any parameters to the experimental data.

In the PPR-78 approach, the Peng-Robinson equation of state[11] (PR EoS) is applied to a mixture of *N* components by use of the van der Waals mixing and combining rules for the attractive parameter *a* and the co-volume parameter *b*:

$$\left.\begin{aligned} a &= \sum_{i=1}^{N}\sum_{j=1}^{N}(1-k_{ij})x_i x_j \sqrt{a_i a_j} \\ b &= \sum_{i=1}^{N} x_i b_i \end{aligned}\right\}, \qquad (6)$$

where k_{ij} is a temperature-dependent binary interaction parameter conventionally fitted to binary VLE data. In the PPR-78 model proposed by Jaubert and co-workers.[20], this binary interaction parameter is obtained according to the following group-contribution formula:

$$k_{ij} = \left[\left\{-\tfrac{1}{2}\sum_{k=1}^{N_g}\sum_{l=1}^{N_g}(\alpha_{ik}-\alpha_{jk})(\alpha_{il}-\alpha_{ji})A_{kl}(T_0 IT)^{(B_{kl}/A_{kl}-1)}\right\} - \left\{\frac{\sqrt{a_i}}{b_i}-\frac{\sqrt{a_j}}{b_j}\right\}\right]\left[2\frac{\sqrt{a_i a_j}}{b_i b_j}\right]^{-1} \qquad (7)$$

Here, N_g is the number of distinguishable functional groups in a given molecule, α_{ik} is the number of occurrences of group *k* in molecule *i* divided by the total number of groups in the molecule, and A_{kl} and B_{kl} are group parameters. Jaubert and co-workers determined these parameters by fitting an extensive database of experimental VLE data. [20, 21, 23, 25]. The phase equilibrium and thermodynamic-property calculations for the PPR-78 mode were carried out in the Aspen Properties software package.[61]

We have also investigated the performance of the SAFT-γ Mie equation of state in comparison with our data.[62] This is also a group-contribution approach wherein the each functional group

is represented by one or more fused heteronuclear segments that interact with a Mie potential. The Mie potential parameters, both like and unlike, have been estimated by regression against experimental data, mainly for pure substances. Typically, the set of experimental data used include vapour pressures, saturated liquid densities (from triple point temperature to approximately 90% of the experimental critical temperature) and compressed-liquid densities (high-pressure region). In cases, such as CO_2, where the molecule is represented as a single group, unlike interaction parameters are obtained from binary VLE and density data. In the present case, the functional groups are aCH, $aCCH_3$ and CO_2 ('a' denotes an aromatic group). The like parameters that characterized these groups were all obtained by Papaioannou et al.,[27] while the unlike parameters have been recently optimised by Al Ghafri et al.,[28] Papaioannou et al.[27] and Dufal et al.[63] Table S12 and S13 in Supporting Information list the values of the parameters used for the individual groups. The computations for SAFT-γ Mie were carried out in gPROMS© software.[64]

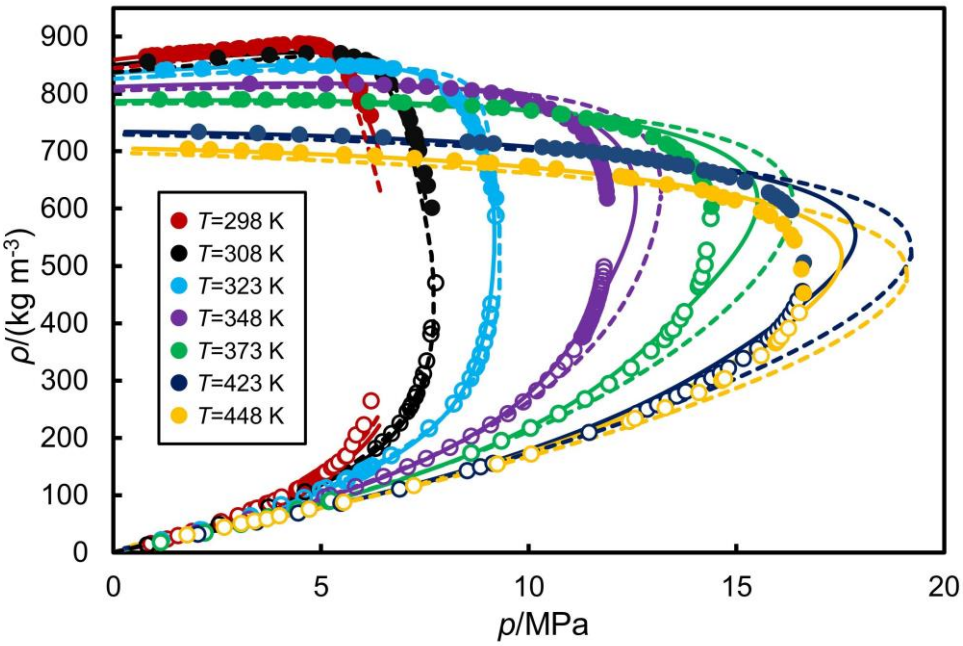

Figure 5. Saturated phase densities, ρ, of ((1−x) C_7H_8+xCO_2) versus pressure, p, at seven temperatures. Symbols represent the experimental values, and dash lines and solid lines the predictions from PPR-78 EoS and SAFT-γ Mie, respectively.

Figure 1 compares the PPR-78 and SAFT-γ Mie predictions for the bubble and dew curves with the experimental data. It can be seen that, while PPR-78 provides a reasonable description of the phase envelope, SAFT-γ Mie is clearly superior, especially in the critical region. As shown in more detail in Figure 2, both models over-predict the critical pressure but SAFT-γ Mie is generally closer to the experimental data. The saturated-phase densities

obtained from the PPR-78 and SAFT-γ Mie models are compared with our results in Figure 5. SAFT-γ Mie predicts the saturated-vapour and saturated-liquid densities well, except in critical region, where the over-prediction of the critical pressure leads to large deviations in density. The dew curve calculated with the PPR-78 model is mostly in good agreement with the experimental data, but the saturated-liquid densities are under-predicted and there are large deviations in the critical region. This result is not surprising as cubic equations are known to provide poor accuracy for liquid densities and the predicted critical locus is substantially in error. It can be concluded from these comparisons that SAFT-γ Mie generally performs better than PPR-78 in the prediction of saturation properties but that neither model is accurate in the critical region.

Figure 6 compares the experimental compressed-fluid densities with values calculated from PPR-78 and SAFT-γ Mie and Figure S7 in the Supporting Information shows the corresponding deviation plots. The PPR-78 EoS generally over-predicts the density on most isotherms but it can be noticed that the predictions improve with increasing CO_2 mole fraction and decreasing pressure. In contrast, SAFT-γ Mie EoS generally under-predicts the density on most isotherms but is generally much more accurate except at high temperatures and high mole fractions of CO_2. The Δ_{AARD} between the experimental data and the predictions of PPR-78 and SAFT-γ Mie are 1.7 % and 1.4 % over the entire measurement range.

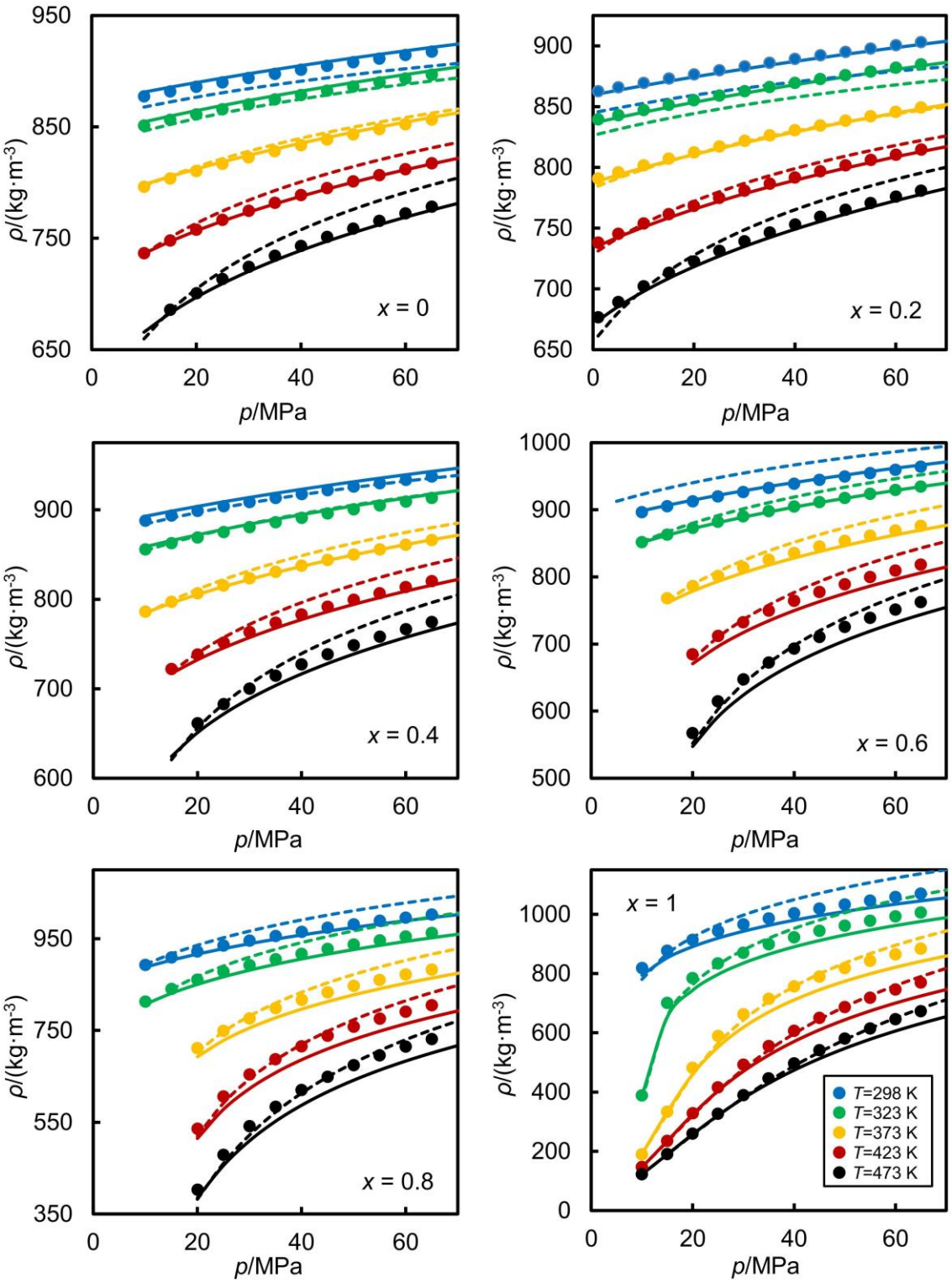

Figure 6. Compress-fluid densities ρ of ((1−x) C_7H_8+xCO_2) system versus pressure p at several temperatures and mole fractions of CO_2. Symbols represent the experimental values, and dash lines and solid lines the predictions from PPR-78 EoS and SAFT-γ Mie, respectively.

The isothermal compressibility, κ_T and the isobaric expansivity, α_p, were calculated by numerical differentiation of ln(ρ) with respect to pressure and temperature, respectively. The results also reported in Tables S5 and S6 in the Supporting Information. Figures 7 and 8 compare the experimentally-derived κ_T and α_p with values calculated from PPR-78 and SAFT-γ Mie. Figure 7 shows that the compressibility predictions of SAFT-γ Mie (Δ_{AARD} = 3 %) are notably better than those of PPR-78 (Δ_{AARD} = 19 %). Figure 8 shows that PPR-78 model performs very poorly for the isobaric expansivities with Δ_{AARD} = 13 % compared with 7 % for SAFT-γ Mie. The performance of SAFT-γ Mie with respect to the derivative properties κ_T and α_p is impressively good and notably better than in the case of the (CO_2 + n-heptane) mixture considered in our earlier work.[18]

Overall, SAFT-γ Mie performs very well in the prediction of VLE, density and derivative properties. It's shortcomings in relation to VLE are mostly a consequence of over-prediction of the critical pressure. SAFT-γ Mie also fails to follow the experimental densities of pure CO_2 at high pressures and temperatures and this situation could probably be improved by re-fitting the parameters taking into account more high-temperature compressed-fluid density data. Furthermore, as discussed by Al Ghafri et al.,[28] the unlike group parameters for CO_2-aCH and CO_2-aCCH_3 were optimised against experimental VLE data only for the (CO_2 + benzene) and (CO_2 + methylbenzene) systems. It seems that the model with optimized parameters is not able to predict density as accurate as the VLE data, especially for the compressed-fluid density. The data reported in the present work could be used to address this issue.

The density predictions of cubic equation of state, such as PPR-78, can be improved at sub-critical temperatures by means of the volume translation method proposed by Peneloux et al.[65] In this context, Privat et al. have studied the effect of the volume translation on mixture properties and they found that by using a linear mixing rule for the volume translation it was possible to predict the liquid densities, phase equilibrium and mixing properties simultaneous.[66] However, in the present case most of the data considered are at temperatures above the critical temperature of CO_2 and these methods do not work well. On the other hand, different mixing rules can be adopted for a better representation of the critical behaviour in binary mixtures. In particular, for CO_2 mixtures, Lasala et al. have studied the combination of the PR equation with residual Helmholtz energy-based mixing rules.[67] They show that this EOS is a reliable approach to calculate the vapour-liquid equilibria of binary mixtures containing CO_2. The authors suggest that this model could be used to represent the thermodynamic properties of multicomponent mixtures in CO_2 capture processes. Therefore, the new data reported herein might be used in the optimisation of CO_2-methylbenzene binary parameters in the model presented by Lasala el al. and extend the equation to (CO_2 + hydrocarbons systems).

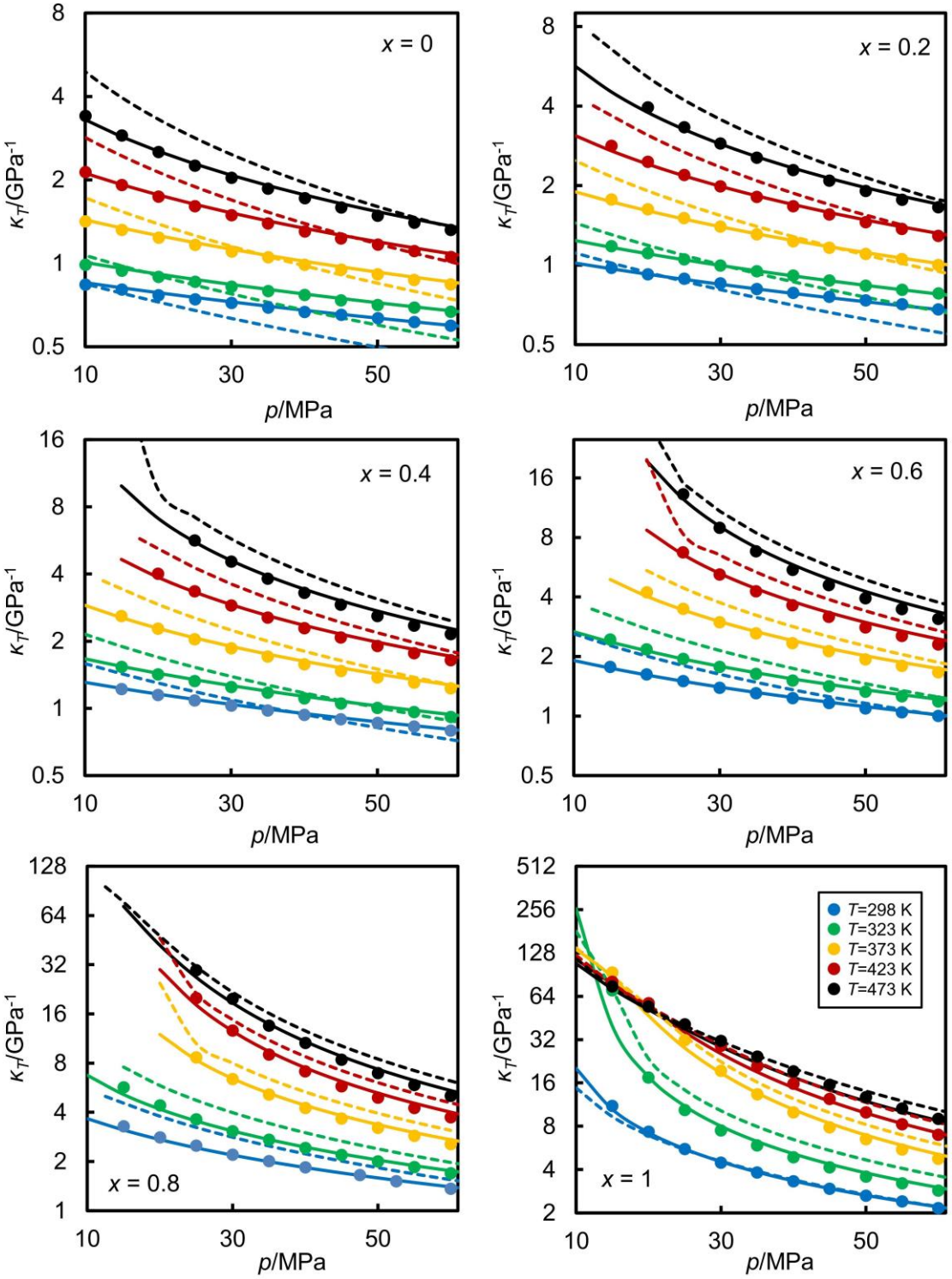

Figure 7. Isothermal compressibilities, κ_T of (1 - x) C_7H_8+x CO_2 versus pressure, *p,* at several temperatures and mole fractions of CO_2. Symbols represent the experimental values, and dash lines and solid lines the predictions from PPR-78 EoS and SAFT-γ Mie, respectively.

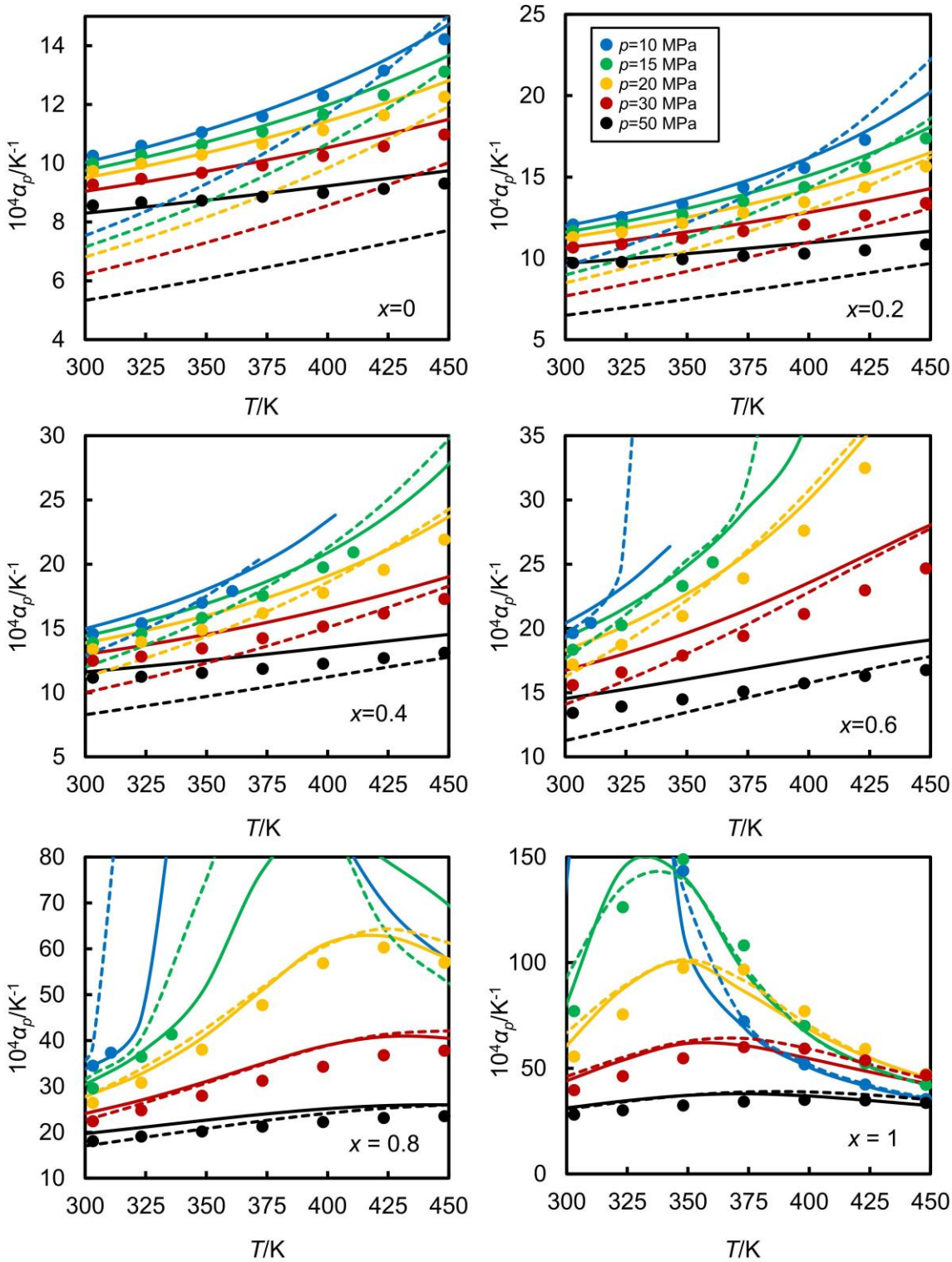

Figure 8. Isobaric expansivities, α_T of (1 - x) C_7H_8+x CO_2 versus temperature, T, at several pressures and mole fractions of CO_2. Symbols represent the experimental values, and dash lines and solid lines the predictions from PPR-78 EoS and SAFT-γ Mie, respectively

Conclusion

In this paper, we report saturated-phase density, compressed-fluid density and VLE data measured over exceptionally-wide ranges of pressure and temperature and across the entire composition range. The estimated standard uncertainty for all density measurements is less than 1.5 $kg \cdot m^{-3}$ throughout the experimental conditions, except for a few points in the critical region. For direct bubble-point measurements, the standard uncertainty was estimated to be 0.1 MPa for most points and less than 0.2 MPa for the critical region. From the data, we have derived excess molar volume, isothermal compressibility and isobaric expansivity. Empirical equations generally represent these data very well and allow useful interpolation and modest extrapolation, including the indirect determination of the bubble-point pressure and density at given temperature and composition.

This comprehensive data set is used to test the performance of two purely-predictive thermodynamic models: PPR-78 and SAFT-γ Mie. These comparisons show generally impressive performance by SAFT-γ Mie in respect of all properties considered, with the main weaknesses being over-prediction of the critical-pressure locus and deviations in the prediction of CO_2 and CO_2-rich mixture densities at high temperatures and pressures.

The properties of the (CO_2 + methylbenzene) mixture studied in this work are found to be quite similar to those of the (CO_2 + n-heptane) system considered previously.[18] However, the present system is characterised by somewhat higher critical pressures, higher densities for both saturated liquid and compressed liquid, and lower compressibility. It also shows more complex non-ideal mixing behaviour at low temperatures, as evidenced by the sigmodal dependence on composition. The phase behaviour of both binary mixtures is generally described well by the two predictive models, except in the critical region. Overall, the two models perform in a similar way for density but SAFT-γ Mie is found to be clearly superior for the isothermal compressibility and isobaric expansivity, especially for the (CO_2 + methylbenzene) system. We believe that there is scope for re-parameterising the SAFT-γ Mie model to better represent properties of CO_2-hydrocarbon systems, especially at conditions of high pressure and high temperature. In contrast, PPR-78 generally performs quite poorly, expect perhaps for VLE, and there appears to be little that can be done to improve it.

Acknowledgements

This research was part of the activities carried out in Qatar Carbonates and Carbon Storage Research Centre (QCCSRC). The authors acknowledge the QCCSRC sponsors: Qatar Petroleum, Shell, and the Qatar Science and Technology and their consent to publish this work. Weparn J Tay is grateful to EPSRC Doctoral Training Award for supporting financially his PhD studies.

Supporting Information

Comparison with literature data for the density measurements. Experimental data: vapour-liquid equilibrium data, saturated phase densities, compressed-fluid densities, isothermal compressibility data and isobaric expansivity data. Parameters of the Redlich-Kister correlation for the excess molar volume. Empirical correlations for the density data. Bubble pressures and bubble compositions obtained from density data. Deviation plots and values of Δ_{AAD} and Δ_{AARD} between the experimental data and the predictions of PPR-78 and SAFT-γ.

References

1. United Nations In *COP21 Paris Agreement*, 2015; 2015.

2. Bataille, C.; Ahman, M.; Neuhoff, K.; Nilsson, L. J.; Fischedick, M.; Lechtenbohmer, S.; Solano-Rodriquez, B.; Denis-Ryan, A.; Stiebert, S.; Waisman, H.; Sartor, O.; Rahbar, S., A review of technology and policy deep decarbonization pathway options for making energy-intensive industry production consistent with the Paris Agreement. *J. Clean. Prod.* **2018,** 187, 960-973.

3. Jarvis, S. M.; Samsatli, S., Technologies and infrastructures underpinning future CO_2 value chains: A comprehensive review and comparative analysis. *Renew. Sust. Energ. Rev.* **2018,** 85, 46-68.

4. Bui, M.; Adjiman, C. S.; Bardow, A.; Anthony, E. J.; Boston, A.; Brown, S.; Fennell, P. S.; Fuss, S.; Galindo, A.; Hackett, L. A.; Hallett, J. P.; Herzog, H. J.; Jackson, G.; Kemper, J.; Krevor, S.; Maitland, G. C.; Matuszewski, M.; Metcalfe, I. S.; Petit, C.; Puxty, G.; Reimer, J.; Reiner, D. M.; Rubin, E. S.; Scott, S. A.; Shah, N.; Smit, B.; Trusler, J. P. M.; Webley, P.; Wilcox, J.; Mac Dowell, N., Carbon capture and storage (CCS): the way forward. *Energy Environ. Sci.* **2018,** 11, (5), 1062-1176.

5. International Energy Agency *World Energy Outlook*; 2018.

6. Edwards, R. W. J.; Celia, M. A., Infrastructure to enable deployment of carbon capture, utilization, and storage in the United States. *Proc. Natl. Acad. Sci. U.S.A.* **2018,** 115, (38), E8815-E8824.

7. Du, F. S.; Nojabaei, B., A review of gas injection in shale reservoirs: enhanced oil/gas recovery approaches and greenhouse gas control. *Energies* **2019,** 12, (12), 33.

8. Eide, L. I.; Batum, M.; Dixon, T.; Elamin, Z.; Graue, A.; Hagen, S.; Hovorka, S.; Nazarian, B.; Nokleby, P. H.; Olsen, G. I.; Ringrose, P.; Vieira, R. A. M., Enabling large-scale carbon capture, utilisation, and storage (CCUS) using offshore carbon dioxide (CO_2) infrastructure developments: a review. *Energies* **2019,** 12, (10).

9. Orr, F. M.; Taber, J. J., Use of carbon-dioxide in enhanced oil-recovery. *Science* **1984,** 224, (4649), 563-569.

10. Bejarano, A.; Simoes, P. C.; del Valle, J. M., Fractionation technologies for liquid mixtures using dense carbon dioxide. *J. Supercrit. Fluids* **2016,** 107, 321-348.

11. Robinson, D. B.; Peng, D.-Y., *The characterization of the heptanes and heavier fractions for the GPA Peng-Robinson programs*. Gas Processors Association: Tulsa, Okla., 1978.

12. Soave, G., Equilibrium constants from a modified Redlich-Kwong equation of state. *Chem. Eng. Sci.* **1972,** 27, (6), 1197-1203.

13. Souza, L. F. S.; Herrig, S.; Span, R.; Trusler, J. P. M., Experimental density and an improved Helmholtz-energy-explicit mixture model for (CO_2 + CO). *Applied Energy* **2019,** 251, 113398.

14. Span, R., *Multiparameter equations of state: an accurate source of thermodynamic property data*. Springer-Verlag: Berlin-Heidelberg, 2000.

15. Nazeri, M.; Chapoy, A.; Burgass, R.; Tohidi, B., Measured densities and derived thermodynamic properties of CO_2-rich mixtures in gas, liquid and supercritical phases from 273K to 423K and pressures up to 126MPa. *J. Chem. Thermodyn.* **2017,** 111, 157-172.

16. Guerrero-Zárate, D.; Estrada-Baltazar, A.; Iglesias-Silva, G. A., Calculation of critical points for natural gas mixtures with the GERG-2008 equation of state. *Fluid Phase Equilib.* **2017,** 437, 69-82.

17. May, E. F.; Guo, J. Y.; Oakley, J. H.; Hughes, T. J.; Graham, B. F.; Marsh, K. N.; Huang, S. H., Reference quality vapor-liquid equilibrium data for the binary systems methane plus ethane, plus propane, plus butane, and +2-methylpropane, at temperatures from (203 to 273) K and pressures to 9 MPa. *J. Chem. Eng. Data* **2015,** 60, (12), 3606-3620.

18. Sanchez-Vicente, Y.; Tay, W. J.; Al Ghafri, S. Z.; Trusler, J. P. M., Thermodynamics of carbon dioxide-hydrocarbon systems. *Applied Energy* **2018,** 220, 629-642.

19. Kandil, M. E.; Al-Saifi, N. M.; Sultan, A. S., Simulation and measurements of volumetric and phase behavior of carbon dioxide plus higher alkanes at high pressure: CO_2 + n-decane at temperatures (313-410) K and pressures up to 76MPa. *Int. J. Greenh. Gas Con.* **2016,** 53, 198-206.

20. Jaubert, J. N.; Mutelet, F., VLE predictions with the Peng-Robinson equation of state and temperature dependent k_{ij} calculated through a group contribution method. *Fluid Phase Equilib.* **2004,** 224, (2), 285-304.

21. Jaubert, J. N.; Privat, R., Relationship between the binary interaction parameters (kij) of the Peng-Robinson and those of the Soave-Redlich-Kwong equations of state: Application to the definition of the PR2SRK model. *Fluid Phase Equilib.* **2010,** 295, (1), 26-37.

22. Vitu, S.; Privat, R.; Jaubert, J. N.; Mutelet, F., Predicting the phase equilibria of CO_2+ hydrocarbon systems with the PPR78 model (PR EOS) and kij calculated through a group contribution method). *J. Supercrit. Fluids* **2008,** 45, (1), 1-26.

23. Jaubert, J. N.; Vitu, S.; Mutelet, F.; Corriou, J. P., Extension of the PPR78 model (predictive 1978, Peng-Robinson EOS with temperature dependent k_{ij} calculated through a

group contribution method) to systems containing aromatic compounds. *Fluid Phase Equilib.* **2005,** 237, (1-2), 193-211.

24. Xu, X.; Jaubert, J.-N.; Privat, R.; Arpentinier, P., Prediction of thermodynamic properties of alkyne-containing mixtures with the E-PPR78 model. *Industrial & Engineering Chemistry Research* **2017,** 56, (28), 8143-8157.

25. Jaubert, J. N.; Privat, R.; Mutelet, F., Predicting the phase equilibria of synthetic petroleum fluids with the PPR78 approach. *AlChE J.* **2010,** 56, (12), 3225-3235.

26. Al Ghafri, S. Z.; Maitland, G. C.; Trusler, J. P. M., Experimental and modeling study of the phase behavior of synthetic crude oil+CO_2. *Fluid Phase Equilib.* **2014,** 365, 20-40.

27. Papaioannou, V.; Calado, F.; Lafitte, T.; Dufal, S.; Sadeqzadeh, M.; Jackson, G.; Adjiman, C. S.; Galindo, A., Application of the SAFT-gamma Mie group contribution equation of state to fluids of relevance to the oil and gas industry. *Fluid Phase Equilib.* **2016,** 416, 104-119.

28. Al Ghafri, S. Z. S.; Maitland, G. C.; Trusler, J. P. M., Phase behavior of the system (carbon dioxide + n-heptane + methylbenzene): A comparison between experimental data and SAFT-γ-Mie predictions. *J. Chem. Eng. Data* **2017,** 62, (9), 2826-2836.

29. Prausnitz, J. M.; Benson, P. R., Solubility of liquids in compressed hydrogen, nitrogen, and carbon dioxide. *AlChE J.* **1959,** 5, (2), 161-164.

30. Ng, H.-J.; Robinson, D. B., Equilibrium-phase properties of the toluene-carbon dioxide system. *J. Chem. Eng. Data* **1978,** 23, (4), 325-327.

31. Sebastian, H. M.; Simnick, J. J.; Lin, H.-M.; Chao, K.-C., Gas-liquid equilibrium in mixtures of carbon dioxide + toluene and carbon dioxide + m-xylene. *J. Chem. Eng. Data* **1980,** 25, (3), 246-248.

32. Chang, C. J.; Chen, C.-Y.; Lin, H.-C., Solubilities of carbon dioxide and nitrous oxide in cyclohexanone, toluene, and N,N-dimethylformamide at elevated pressures. *J. Chem. Eng. Data* **1995,** 40, (4), 850-855.

33. Tochigi, K.; Hasegawa, K.; Asano, N.; Kojima, K., Vapor-liquid equilibria for the carbon dioxide + pentane and carbon dioxide + toluene systems. *J. Chem. Eng. Data* **1998,** 43, (6), 954-956.

34. Lazzaroni, M. J.; Bush, D.; Brown, J. S.; Eckert, C. A., High-pressure vapor−liquid equilbria of some carbon dioxide + organic binary systems. *J. Chem. Eng. Data* **2005,** 50, (1), 60-65.

35. Lay, E. N.; Taghikhani, V.; Ghotbi, C., Measurement and correlation of CO_2 solubility in the systems of CO_2 + Toluene, CO_2 + Benzene, and CO_2 + n-Hexane at near-critical and supercritical conditions. *J. Chem. Eng. Data* **2006,** 51, (6), 2197-2200.

36. Naidoo, P.; Ramjugernath, D.; Raal, J. D., A new high-pressure vapour–liquid equilibrium apparatus. *Fluid Phase Equilib.* **2008,** 269, (1), 104-112.

37. Kim, C. H.; Vimalchand, P.; Donohue, M. D., Vapor-liquid-equilibria for binary-mixtures of carbon-dioxide with benzene, toluene and para-xylene. *Fluid Phase Equilib.* **1986,** 31, (3), 299-311.

38. Fink, S. D.; Hershey, H. C., Modeling the vapor-liquid-equilibria of 1,1,1-trichloroethane + carbon-dioxide and toluene + carbon-dioxide at 308 K, 323 K, and 353 K. *Ind. Eng. Chem. Res.* **1990,** 29, (2), 295-306.

39. Zilnik, L. F.; Grilc, M.; Levec, J.; Peper, S.; Dohrn, R., Phase-equilibrium measurements with a novel multi-purpose high-pressure view cell: CO_2 + n-decane and CO_2 + toluene. *Fluid Phase Equilib.* **2016,** 419, 31-38.

40. Lay, E. N., Measurement and correlation of bubble point pressure in (CO_2 + C_6H_6), (CO_2 + $CH_3C_6H_5$), (CO_2 + C_6H_{14}), and (CO_2 + C_7H_{16}) at temperatures from (293.15 to 313.15) K. *J. Chem. Eng. Data* **2010,** 55, (1), 223-227.

41. Wu, W.; Ke, J.; Poliakoff, M., Phase boundaries of CO_2 + toluene, CO_2 + acetone, and CO_2 + ethanol at high temperatures and high pressures. *J. Chem. Eng. Data* **2006,** 51, (4), 1398-1403.

42. Pohler, H.; Kiran, E., Volumetric properties of carbon dioxide plus toluene at high pressures. *J. Chem. Eng. Data* **1996,** 41, (3), 482-486.

43. Wu, J. L.; Pan, Q. M.; Rempel, G. L., Pressure-density-temperature behavior of CO_2+acetone, CO_2+toluene, and CO_2+monochlorobenzene mixtures in the near-critical region. *J. Chem. Eng. Data* **2004,** 49, (4), 976-979.

44. Zirrahi, M.; Azinfar, B.; Hassanzadeh, H.; Abedi, J., Measuring and Modeling the Solubility and Density for CO_2-Toluene and C_2H_6-Toluene Systems. *J. Chem. Eng. Data* **2015,** 60, (6), 1592-1599.

45. Efika, E. C.; Hoballah, R.; Li, X. S.; May, E. F.; Nania, M.; Sanchez-Vicente, Y.; Trusler, J. P. M., Saturated phase densities of (CO_2 + H_2O) at temperatures from (293 to 450) K and pressures up to 64 MPa. *J. Chem. Thermodyn.* **2016,** 93, 347-359.

46. Al Ghafri, S. Z. S.; Trusler, J. P. M., Phase equilibria of (Methylbenzene + Carbon dioxide + Methane) at elevated pressure: Experiment and modelling. *J. Supercrit. Fluid,* **2019,** 145, 1-9.

47. Tay, W. J.; Trusler, J. P. M., Density, sound speed and derived thermophysical properties of n-nonane at temperatures between (283.15 and 473.15) K and at pressures up to 390 MPa. *J. Chem. Thermodyn.* **2018,** 124, 107-122.

48. Kwon, C. H.; Seo, M. D.; Kim, S. W.; Lee, C. S.; Kang, J. W., Vapor-liquid equilibrium for carbon dioxide plus isopropyl, isobutyl, and isoamyl acetates. *J. Chem. Eng. Data* **2007,** 52, (3), 727-730.

49. Lemmon, E. W.; Span, R., Short fundamental equations of state for 20 industrial fluids. *J. Chem. Eng. Data* **2006,** 51, (3), 785-850.

50. May, E. F.; Tay, W. J.; Nania, M.; Aleji, A.; Al-Ghafri, S.; Trusler, J. P. M., Physical apparatus parameters and model for vibrating tube densimeters at pressures to 140 MPa and temperatures to 473 K. *Rev. Sci. Instrum.* **2014,** 85, (9).

51. May, E. F.; Tay, W. J.; Nania, M.; Aleji, A.; Al-Ghafri, S.; Trusler, J. P. M., Physical apparatus parameters and model for vibrating tube densimeters at pressures to 140 MPa and temperatures to 473 K (vol 85, 095111, 2014). *Rev. Sci. Instrum.* **2015,** 86, (4).

52. Wagner, W.; Pruss, A., The IAPWS formulation 1995 for the thermodynamic properties of ordinary water substance for general and scientific use. *J. Phys. Chem. Ref. Data* **2002,** 31, (2), 387-535.

53. Ortiz-Vega, D. O. A New Wide Range Equation Of State For Helium-4. Texas A&M University, 2013.

54. Ortiz-Vega, D. O.; Hall, K. R.; Holste, J. C.; Arp, V. D.; Harvey, A. H.; Lemmon, E. W., A New Wide Range Equation Of State For Helium-4. *J. Phys. Chem. Ref. Data* **2018,** (To be published).

55. JCGM *Uncertainty of measurement - Part 3: Guide to the expression of uncertainty in measurement (GUM:1995).* ; 2008.

56. Span, R.; Wagner, W., A new equation of state for carbon dioxide covering the fluid region from the triple-point temperature to 1100 K at pressures up to 800 MPa. *J. Phys. Chem. Ref. Data* **1996,** 25, (6), 1509-1596.

57. Ziegler, J. W.; Chester, T. L.; Innis, D. P.; Pages, S. H.; Dorsey, J. G., Supercritical fluid flow injection method for mapping liquid-vapor critical loci of binary mixtures containing CO_2. In *Innovations in Supercritical Fluids: Science and Technology*, Hutchenson, K. W.; Foster, N. R., Eds. 1995; Vol. 608, pp 93-110.

58. Heidemann, R. A.; Khalil, A. M., The calculation of critical-points. *AlChE J.* **1980,** 26, (5), 769-779.

59. Privat, R.; Jaubert, J.-N., Classification of global fluid-phase equilibrium behaviors in binary systems. *Chem. Eng. Res. Des.* **2013,** 91, (10), 1807-1839.

60. van Konynenburg, P. H.; Scott, R. L., Critical lines and phase equilibriums in binary Van der Waals mixtures. *Philos. Trans. Royal Soc. A* **1980,** 298, (1442), 495-540.

61. Chamorro, C. R.; Segovia, J. J.; Martin, M. C.; Villamanan, M. A.; Estela-Uribe, J. F.; Trusler, J. P. M., Measurement of the (pressure, density, temperature) relation of two (methane + nitrogen) gas mixtures at temperatures between 240 and 400 K and pressures up to 20 MPa using an accurate single-sinker densimeter. *J. Chem. Thermodyn.* **2006,** 38, (7), 916-922.

62. Papaioannou, V.; Lafitte, T.; Avendaño, C.; Adjiman, C. S.; Jackson, G.; Müller, E. A.; Galindo, A., Group contribution methodology based on the statistical associating fluid theory for heteronuclear molecules formed from Mie segments. *J. Chem. Phys.* **2014,** 140, (5), 054107.

63. Dufal, S.; Papaioannou, V.; Sadeqzadeh, M.; Pogiatzis, T.; Chremos, A.; Adjiman, C. S.; Jackson, G.; Galindo, A., Prediction of thermodynamic properties and phase behavior of fluids and mixtures with the SAFT-γ Mie group-contribution equation of state. *J. Chem. Eng. Data* **2014,** 59, (10), 3272-3288.

64. Estela-Uribe, J. F.; Trusler, J. P. M.; Chamorro, C. R.; Segovia, J. J.; Martin, M. C.; Villamanan, M. A., Speeds of sound in {(1-x)CH_4+ xN_2} with x = (0.10001, 0.19999, and 0.5422) at temperatures between 170 K and 400 K and pressures up to 30 MPa. *J. Chem. Thermodyn.* **2006,** 38, (7), 929-937.

65. Péneloux, A.; Rauzy, E.; Fréze, R., A consistent correction for Redlich-Kwong-Soave volumes. *Fluid Phase Equilib.* **1982,** 8, (1), 7-23.

66. Privat, R.; Jaubert, J.-N.; Le Guennec, Y., Incorporation of a volume translation in an equation of state for fluid mixtures: which combining rule? which effect on properties of mixing? *Fluid Phase Equilib.* **2016,** 427, 414-420.

67. Lasala, S.; Chiesa, P.; Privat, R.; Jaubert, J.-N., Modeling the Thermodynamics of Fluids Treated by CO2 Capture Processes with Peng–Robinson + Residual Helmholtz Energy-Based Mixing Rules. *Industrial & Engineering Chemistry Research* **2017,** 56, (8), 2259-2276.

Table of Contents and Abstract Graphics